PHOTONICS Research

Physical conversion and superposition of optical skyrmion topologies

Houan Teng,[1] Jinzhan Zhong,[1,2] Jian Chen,[1,2] Xinrui Lei,[1,2] and Qiwen Zhan[1,2,*]

[1]School of Optical-Electrical and Computer Engineering, University of Shanghai for Science and Technology, Shanghai 200093, China
[2]Zhangjiang Laboratory, Shanghai 201204, China
*Corresponding author: qwzhan@usst.edu.cn

Received 4 July 2023; revised 1 October 2023; accepted 2 October 2023; posted 4 October 2023 (Doc. ID 499485); published 22 November 2023

Optical skyrmions are quasiparticles with nontrivial topological textures that have significant potential in optical information processing, transmission, and storage. Here, we theoretically and experimentally achieve the conversion of optical skyrmions among Néel, Bloch, intermediate skyrmions, and bimerons by polarization devices, where the fusion and annihilation of optical skyrmions are demonstrated accordingly. By analyzing the polarization pattern in Poincaré beams, we reveal the skyrmion topology dependence on the device, which provides a pathway for the study of skyrmion interactions. A vectorial optical field generator is implemented to realize the conversion and superposition experimentally, and the results are in good agreement with the theoretical predictions. These results enhance our comprehension of optical topological quasiparticles, which could have a significant impact on the transfer, storage, and communication of optical information.

https://doi.org/10.1364/PRJ.499485

1. INTRODUCTION

Skyrmions are topologically protected quasiparticles originating from high-energy and condensed matter physics [1], and they hold great promise for future applications in spintronics, information processing, and high-density data storage due to their ultracompact size, topology-protected stability, and low current requirements [2–5]. Recently, the photonic counterpart of magnetic skyrmions was observed in either guided waves or paraxial vector beams. On the one hand, the 2D confinement of light in guided waves provides a smooth domain for skyrmion generation, which can be constructed by electric/magnetic field and spin angular momentum [6–17], with the topology constrained by the symmetry of a field. On the other hand, skyrmions formed with Stokes parameters corresponding to a spatial variation of a polarization pattern was proposed in paraxial vector beams [18–22] or microcavity [23–26], where the topological feature is manipulated by the selection of Poincaré beams. The variety of structured vector beams inspires a significant effort to investigate more kinds of optical quasiparticles, such as multiple π-twist target skyrmion, antiskyrmions and bimerons [27,28]. In addition, the electromagnetic fields supertoroidal pulses also exhibit skyrmionic structure [29,30]. The ultrasmall and ultrafast characteristics of optical skyrmions have demonstrated advanced applications in superresolution imaging, metrology, and light–matter interactions [12,29–32].

While various skyrmionic textures have been demonstrated in optics, the generation and manipulation of Stokes skyrmions rely on digital hologram method assisted by spatial light modulator [19,22,33]. The conversion between different topologies upon propagation and diffraction has not yet been achieved, which is important for skyrmion dynamics and interactions. The wave plate (WP) is a fundamental optical component extensively employed in polarization optics and facilitates the manipulation of polarization states without changing the amplitude of the optical field [34,35]. The Stokes vector provides a valuable representation of polarization states, making the WP an essential tool for skyrmion conversion without altering the skyrmion number.

In this work, we proposed a method to realize the homogeneous conversion between skyrmions, including Néel, Bloch, intermediate skyrmion types, and bimerons (topological quasiparticle homeomorphic to skyrmions), and explored the superposition of skyrmionic textures. We have theoretically derived the Mueller matrix of devices to achieve the conversion of skyrmions topology, which we identify as a series of WPs. With the conversion between different skyrmionic textures, the skyrmion number remains invariant, manifesting the topological protection. More significantly, we have experimentally verified the conversion by implementing a vectorial optical field generator, which showed good agreement with theoretical predictions. Based on the conversion between skyrmions, the fusion and annihilation of optical skyrmions were demonstrated by their superpositions. This work lays the foundation for exploiting the potential of topological photonics in the fields of optical signal processing and information transmission.

2. THEORY

A. Optical Topological Quasiparticle

Optical topology quasiparticle can be formed by the Stokes vectors of a Poincaré beam composed of a pair of Laguerre–Gaussian (LG) modes with orthogonal polarization states, which can be expressed as [18,36]

$$\Psi = \cos\, c_0 \cdot \mathrm{LG}_{0,0}\vec{e}_0 + \sin\, c_0 \cdot e^{i\phi_\gamma}\mathrm{LG}_{0,l}\vec{e}_1, \tag{1}$$

where $\vec{e}_0, \vec{e}_1$ represent orthogonal polarization states, and $\mathrm{LG}_{p,l}$ is the Laguerre–Gaussian mode [37] characterized by radial and azimuthal indices (p, l). The global phase difference between the two orthogonal polarization components is denoted by ϕ_γ, which controls the helicity textures of topological quasiparticle. c_0 is a constant that controls the amplitude ratio of the orthogonal modes.

Selecting the eigenstates as circular polarization $(\vec{e}_0, \vec{e}_1) = (\vec{e}_R, \vec{e}_L)$, the normalized Stokes vector can be expressed as

$$\vec{s} = \begin{pmatrix} \cos\,\beta(\rho)\cos\,\alpha(\phi) \\ \cos\,\beta(\rho)\sin\,\alpha(\phi) \\ \sin\,\beta(\rho) \end{pmatrix}, \tag{2}$$

where $\cos\,\beta(\rho) = \frac{2\rho}{1+\rho^2}$, $\sin\,\beta(\rho) = \frac{1-\rho^2}{1+\rho^2}$, $\rho(r) = \tan\, c_0 \cdot (\frac{\sqrt{2}r}{w_0})^{|l|}$, and $\alpha(\phi) = l\phi + \phi_\gamma$.

The Stokes vector in Eq. (2) describes a mapping to the unit sphere, which represents the swirling structure of a skyrmion [1,2]. The topological property of an optical skyrmion is determined by the skyrmion number, which represents the number of times the Stokes vector wraps around a unit sphere, expressed as

$$N_s = \frac{1}{4\pi}\iint \vec{s}\cdot\left(\frac{\partial\vec{s}}{\partial x}\times\frac{\partial\vec{s}}{\partial y}\right)\mathrm{d}x\mathrm{d}y. \tag{3}$$

Considering the radial symmetry, the skyrmion number can be calculated through $N_s = p\cdot m = \frac{1}{2}[\sin\,\beta(r)]_{r=0}^{r=r_\sigma}\cdot\frac{1}{2\pi}[\alpha(\phi)]_{\phi=0}^{\phi=2\pi}$ [1,2,38] (see Appendix A for details). The polarity p can be expressed as $p = \frac{1}{2}[\sin\,\beta(\rho)]_{r=0}^{r=r_\sigma}$, describing the variation of out-of-plane Stokes vector orientation. The vorticity m is expressed in terms of the integer $m = \frac{1}{2\pi}[\alpha(\phi)]_{\phi=0}^{\phi=2\pi}$ describing the in-plane Stokes vector orientation, which is equal to the topological charge l of $\mathrm{LG}_{0,l}$. The offset ϕ_γ of $\alpha(\phi) = l\phi + \phi_\gamma$ is the helicity representing the initial phase of Stokes vector orientation.

The skyrmion topology is determined by the polarity, vorticity, and helicity. The helicity of optical quasiparticle controls the orientation of Stokes vector in the S_1–S_2 plane (skyrmion) or S_2–S_3 plane (bimeron) corresponding to the global phase difference between orthogonal polarization states. The topological quasiparticle is classified as Néel-type with $\phi_\gamma = 0, \pi$ [39], and as Bloch-type with $\phi_\gamma = \pm\pi/2$ [40,41]. The polarity of optical quasiparticle controls the out-of-plane Stokes vector orientation, which corresponds to Stokes vector s_3. For $p = 1$ ($p = -1$), the orientation of Stokes vector is downward (upward) at the center and upward (downward) at the boundary. The vorticity determined by l controls the distribution of the transverse Stokes vector orientation. As $l = -1$ antiskyrmions with saddle textures are formed [42]. According to the relationship of the Stokes vector, we can achieve the conversion between optical skyrmions with different helicity, opposite polarity (with simultaneous opposite vorticity), and even bimeron by employing optical WPs, which reveals different mapping from the finite plane (representing the normal skyrmion configuration) to the Poincaré sphere, as illustrated in Fig. 1.

B. Conversion of Optical Skyrmion by Optical Devices

In Section 2.A, we have demonstrated the skyrmion topology dependence on the property of structured vector beam, which enables the conversion of different topological quasiparticles using optical devices, as expressed by the equation

$$s_{\mathrm{out}} = M \cdot s_{\mathrm{in}}, \tag{4}$$

where s_{in} is the Stokes vector field configuration of the initial topological texture, M is Mueller matrices of optical devices, which can consist of one or more wave plates, and s_{out} is the Stokes vector field configuration of output topological texture. The fundamental theory of the skyrmion conversion is given in Appendix B.

First, we examine the conversion of skyrmions with different helicity. Skyrmions with different helicities, such as Néel, Bloch, and intermediate types, exhibit distinct orientations of the Stokes vector in the S_1–S_2 plane, which are controlled by the parameter ϕ_γ, as described in Eq. (2). Without loss of generality, we consider the input type as a Néel skyrmion with $\phi_\gamma = 0$. It has been demonstrated that the Stokes vector of a structured light can be tuned by an optical polarization rotator (PR) [43]. The PR is composed of two crossed quarter-wave plates (QWPs) with fast axes at 0 and $\pi/2$ and a retarder with fast axis at $\pi/4$ (phase delay of ϕ_d) positioned between them. The Mueller matrices of the PR are given by

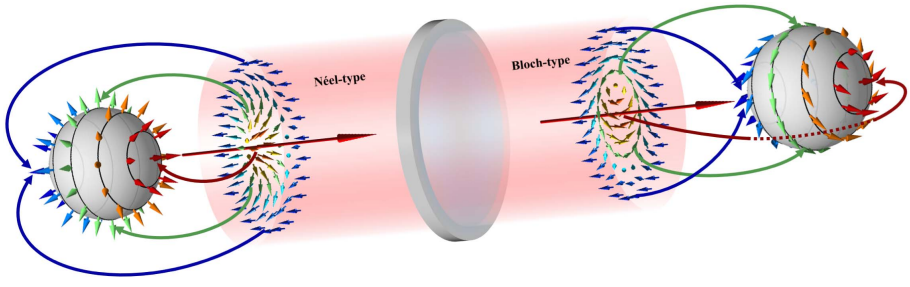

Fig. 1. Schematic diagram of the conversion of optical topological quasiparticle with polarization devices.

$$M_{\mathrm{PR}}(\phi_d/2) = M_{\mathrm{QWP}}(\pi/2)M_{\mathrm{WP}}(\phi_d,\pi/4)M_{\mathrm{QWP}}(0) = \begin{bmatrix} \cos\phi_d & -\sin\phi_d & 0 \\ \sin\phi_d & \cos\phi_d & 0 \\ 0 & 0 & 1 \end{bmatrix}. \quad (5)$$

By substituting Eq. (5) into Eq. (4), the output Stokes vector field configuration can be written as

$$s_{\mathrm{out}} = M_{\mathrm{PR}}(\phi_d/2)\cdot s_{\mathrm{in}} = \begin{pmatrix} \cos\beta(\rho)\cos(l\phi+\phi_d) \\ \cos\beta(\rho)\sin(l\phi+\phi_d) \\ \sin\beta(\rho) \end{pmatrix}, \quad (6)$$

demonstrating that a PR with a rotation of $\phi_d/2$ can induce a rotation of ϕ_d in the helicity of optical skyrmions while keeping the polarity and vorticity unchanged. Therefore, the skyrmion number remains constant. Figure 2(a) shows the input skyrmion of Néel type with $l = 1$ and $\phi_\gamma = 0$, and the three components of Stokes vector are depicted in the inset of Fig. 2. By employing a PR with a rotation of $\pi/4$, the spatial configuration of Stokes parameters s_1 and s_2 performs a clockwise rotation of $\pi/2$, while the corresponding Stokes vector undergoes a counterclockwise rotation, resulting in the generation of a Bloch skyrmion with $\phi_\gamma = \phi_d = \pi/2$, as shown in Fig. 2(b). Thus, the helicity texture of optical skyrmions can be fully controlled by adjusting the phase delay of the retarder of the PR. Furthermore, the utilization of an electrically adjustable retardance as a retarder enables rapid conversion between skyrmion types, thereby presenting potential applications in areas like optical signal processing and information transfer.

The helicity of optical skyrmion can be adjusted with the employment of PR. We further explore the conversion of the polarity of optical skyrmion. The polarity describes the variation of out-of-plane Stokes vector orientation, which is calculated by $p = \frac{1}{2}[\sin\beta(\rho)]_{r=0}^{r=r_\sigma} = \frac{1}{2}[\frac{1-\rho^2(r)}{1+\rho^2(r)}]_{r=0}^{r=r_\sigma}$, where $\rho = \tan c_0 \cdot (\frac{\sqrt{2}r}{w_0})^{|l|}$ represents the amplitude ratio of left- and right-handed polarized components. Consequently, as the ratio changes from ρ to $1/\rho$, the polarity p is converted from 1 to −1. This conversion can be achieved using only a single half-wave plate (HWP) as the initial type is set as a Néel skyrmion with $\phi_\gamma = 0$, resulting in the derived output skyrmion as

$$s_{\mathrm{out}} = M_{\mathrm{HWP}}(0)\cdot s_{\mathrm{in}} = \begin{pmatrix} \cos(-\beta)\cos(-l\phi) \\ \cos(-\beta)\sin(-l\phi) \\ \sin(-\beta) \end{pmatrix}. \quad (7)$$

It is worth noting that the HWP not only reverses the orientation of the out-of-plane Stokes vector s_3 but also changes the in-plane Stokes vector S_2, resulting in modulation on the vorticity of skyrmion. The Stokes vector field configuration of the output skyrmion is shown in Fig. 2(c), exhibiting an antiskyrmion. In this case, the polarity and vorticity are reversed, while the skyrmion number remains invariant, manifesting the topological protection of skyrmions.

Finally, we investigate the conversion between skyrmions and skyrmion-homeomorphic quasiparticles, referred to as "homeomorphic conversion." By employing two WPs with fast axes aligned at $-\pi/4$ and $\pi/2$, skyrmions can be converted into bimerons. The Mueller matrix for this conversion can be represented as

$$M_{\mathrm{QQ}} = M_{\mathrm{QWP}}(\pi/2)M_{\mathrm{QWP}}(-\pi/4) = \begin{bmatrix} 0 & 0 & 1 \\ 1 & 0 & 0 \\ 0 & 1 & 0 \end{bmatrix}. \quad (8)$$

Thus, the output type of skyrmion can be written as

$$s_{\mathrm{out}} = M_{\mathrm{QQ}}\cdot s_{\mathrm{in}} = \begin{pmatrix} \sin\beta(\rho) \\ \cos\beta(\rho)\cos(l\phi+\phi_\gamma) \\ \cos\beta(\rho)\sin(l\phi+\phi_\gamma) \end{pmatrix}. \quad (9)$$

Equation (9) represents quasiparticles known as bimerons, which are homeomorphic to skyrmions, by applying linear polarization $(\vec{e}_0,\vec{e}_1) = (\vec{e}_X,\vec{e}_Y)$ as eigenstates, as described in Eq. (1). According to Eq. (9), the three components of the Stokes vector change from $(s_1,s_2,s_3)^T$ to $(s_3,s_1,s_2)^T$, but this does not affect its skyrmion number because it still covers the Poincaré sphere only once. As the initial type is Néel skyrmion

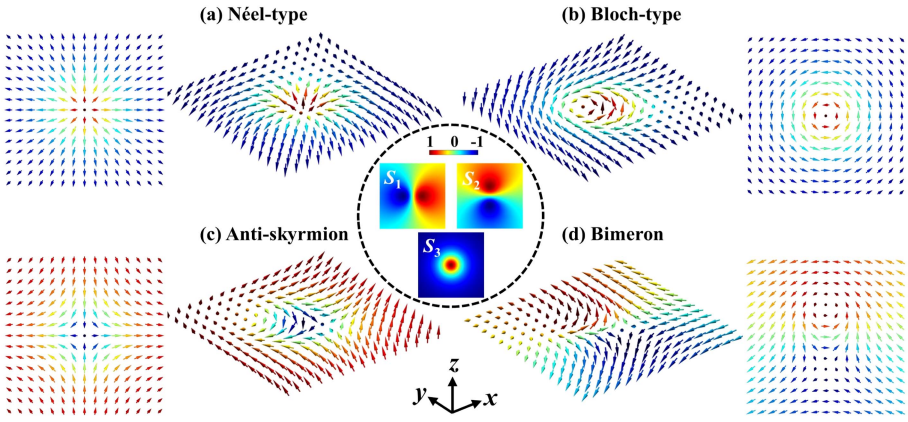

Fig. 2. Simulation results for optical skyrmion conversion with polarization devices. (a) Input Stokes vector configuration and transverse component of Néel skyrmion. Output Stokes vector configuration and transverse component of (b) Bloch skyrmion converted by PR, (c) antiskyrmion with $p = -1$ converted by HWP, and (d) bimeron converted by two QWPs. The Stokes parameters for input skyrmion are shown inside the dashed circle.

with $l = 1$ and $\phi_\gamma = 0$, the field configuration of output Stokes vector is as shown in Fig. 2(d).

3. EXPERIMENT AND DISCUSSION

In order to investigate the conversion of optical skyrmions, a vectorial optical field generator [44] was constructed, as depicted in Fig. 3, which is capable of generating optical skyrmions. The setup utilizes two spatial light modulators (SLMs) divided into four sections to precisely control the phase, amplitude, polarization ratio, and retardation of vectorial optical fields [44]. A He–Ne laser beam was employed as the input light source, and the intensity of the Gaussian beam was regulated using a polarizer and an HWP. The beam was subsequently directed through SLM Section 1, where its phase was directly modulated. The phase-modulated beam was then projected onto SLM Section 2, which served as a PR in conjunction with a QWP and polarizer to modulate the beam's amplitude. The second 4-f imaging system projected the horizontally polarized beam with the desired amplitude and phase onto SLM Section 3, where the polarization ratio was further adjusted using another PR constructed from a QWP and SLM Section 3. Subsequently, this beam traversed SLM Section 4 to regulate retardation by manipulating only the phase of the horizontal polarization component. The optical skyrmion was constructed and then passed through the skyrmion convertor to achieve the conversion. Finally, the conversed optical skyrmion was imaged on the CCD via the last 4-f imaging system. It is worth noting that optical Stokes skyrmions can also be experimentally generated using alternative vectorial optical field generators, such as splitting a single SLM into two parts to independently modulate the complex amplitudes of two orthogonal polarizations [19].

Our vectorial optical field generator facilitates the generation of Stokes skyrmions with customizable polarity and helicity topology texture, as described by Eq. (1). In order to experimentally reconstruct an optical skyrmion, the Stokes parameters S_0, S_1, S_2, and S_3 were obtained by measuring the intensity of various polarization components. The relationship between Stokes parameters and individual polarization component intensities can be expressed as follows:

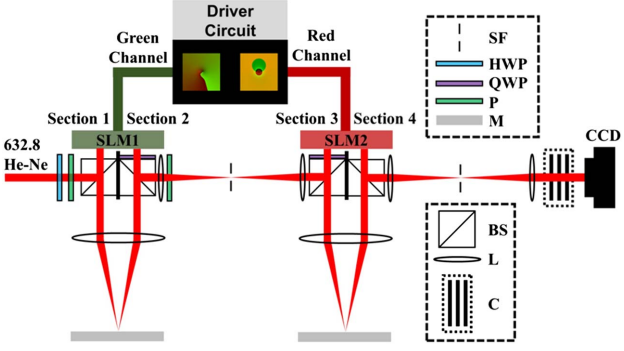

Fig. 3. Schematic diagram of the vectorial optical field generator. SLM, spatial light modulator; SF, spatial filter; HWP, half-wave plate; QWP, quarter-wave plate; P, polarizer; M, mirror; BS, beam splitter; L, lens; C, optical skyrmion converter.

$$\begin{aligned} S_0 &= I(0,0) + I(\pi/2,\pi/2), \\ S_1 &= I(0,0) - I(\pi/2,\pi/2), \\ S_2 &= I(\pi/4,\pi/4) - I(-\pi/4,\ -\pi/4), \\ S_3 &= I(\pi/4,0) - I(-\pi/4,0), \end{aligned} \tag{10}$$

where $I(\theta_1,\theta_2)$ represents the optical intensity after passing through a QWP at θ_1 and a polarizer at θ_2.

A. Conversion of Optical Skyrmion

While it is feasible to experimentally generate various types of optical skyrmions by manipulating their polarity, vorticity, and helicity, there is currently a lack of solutions to implement interconversion between different types of skyrmions. Based on the aforementioned investigation, we have theoretically demonstrated that this conversion can be accomplished through the utilization of fundamental WPs called an "optical skyrmion converter." In our study, we have performed an experimental demonstration showcasing the capability to convert between different types of optical skyrmions. The input in our experiment was an optical field that exhibited a classical Néel skyrmion topology. For the conversion process, we employed a specifically designed optical skyrmion converter comprising QWPs and an HWP, which are elaborated on in Section 2. Subsequently, the output skyrmion was detected and analyzed using a polarization analyzer (PA) consisting of a QWP and a polarizer.

We have designed an optical skyrmion converter to experimentally achieve the conversion between different types of skyrmions. First, we present the conversion of optical skyrmions with different helicity. By superposing a pair of orthogonally polarized LG modes, we can experimentally create a fundamental Néel skyrmion of $p = 1$, $l = 1$, and $\phi_\gamma = 0$, as shown in Fig. 4(a). To convert the helicity of optical skyrmion, we adjust the rotation angle of PR from 0 to $\pi/4$. As a result, the Néel skyrmion with $\phi_\gamma = 0$ evolves into a Bloch skyrmion with $\phi_\gamma = \pi/2$ [Fig. 4(b)]. The Stokes vector performs a $\pi/2$ rotation counterclockwise around the S_3 axis. The Stokes vector S_3 remains constant [Fig. 4(b1)], preserving the polarity, while s_1 and s_2 take a $\pi/2$ rotation counterclockwise in S_1–S_2 plane, which does not change the vorticity [Fig. 4(b2)], indicating the topological protection of skyrmionic textures. The invariance of the skyrmion number is further confirmed through numerical integration, as described in Eq. (3), using the experimental results shown in Figs. 4(a) and 4(b). The experimental errors in skyrmion number arise from the limited numerical aperture of the experimental system and system noise fluctuations, especially in low-intensity regions [45]. Note that, if the rotation angle of PR is π, the optical skyrmion will revert back to a Néel skyrmion. In this demonstration, we specifically show the conversion using a PR with a rotation angle of $\pi/4$, but the same principle can be applied to achieve arbitrary helicity conversion by using a PR with the corresponding rotation angle.

It is important to note that Néel, Bloch, and intermediate skyrmions can naturally evolve into each other due to the different Gouy phase shifts between two orthogonal spatial modes, but this requires a long propagation distance [18,28]. For example, to achieve this conversion between Néel and Bloch types, it requires at least one Rayleigh distance (for a laser with

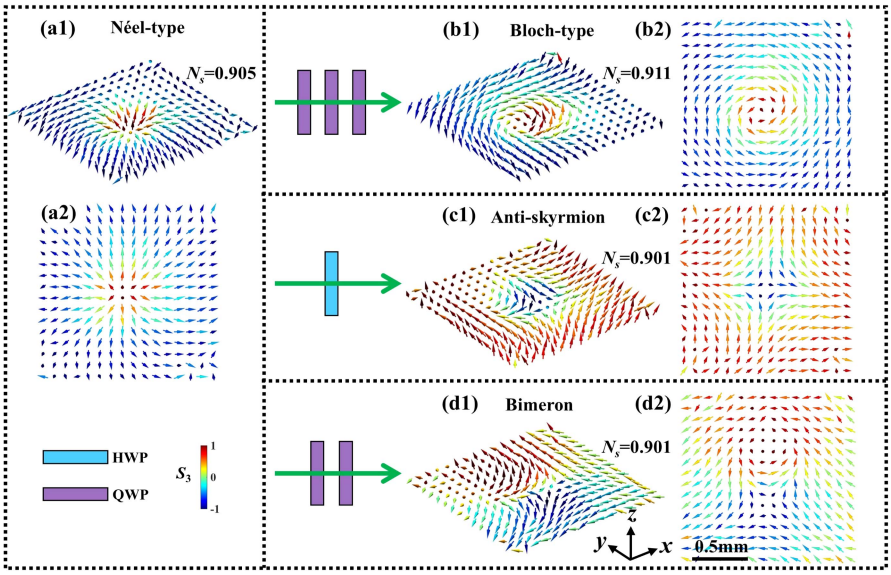

Fig. 4. Experimental results for optical skyrmion conversion. (a) Input Néel skyrmion and top view below. Output Stokes vector of (b) Bloch skyrmion converted by PR, (c) anti-skyrmion with $p = -1$ converted by HWP, and (d) bimeron converted by two QWPs with top view of the skyrmionic texture right. Numerically calculated skyrmion numbers are indicated in their respective panels.

a wavelength of 633 nm and a beam waist radius of 1 mm, this corresponds to approximately 5 m). In our approach, the distance limitation depends on the thickness of the WP combination, which typically remains within 10 cm. Our methods offer the advantages of a short conversion distance, ease of control, and cost-effectiveness, making them relevant for future applications in optical communication and optical information storage.

To convert the polarity of the optical skyrmion, we utilize an HWP to convert the Néel skyrmion to antiskyrmion with $p = -1$, as depicted in Fig. 4(c). The Stokes vector performs a π clockwise rotation around the S_1 axis. As a result, the Stokes vector s_1 remains constant, while s_2 is reversed [Fig. 4(c2)], leading to a change in vorticity from 1 to −1. Additionally, the Stokes vector s_3 undergoes a reversal [Fig. 4(c1)], resulting in a reversal of the polarity. As previously discussed in the theoretical section, the HWP not only reverses the polarity but also the vorticity while keeping the skyrmion number invariant, as shown in Figs. 4(a) and 4(c). By adjusting the rotation angle of PR, we can effectively convert the helicity and obtain similar outcomes to those presented in Fig. 4(b) but with an opposite polarity. It is worth noting that, despite slight deviations in the optical field, the type of skyrmion remains unaffected.

Skyrmions and bimerons are two types of optical quasiparticles characterized by homeomorphic topological textures. To achieve the homeomorphic conversion, we apply two QWPs with a fast axis at $-\pi/4$ and $\pi/2$ to modulate the Néel skyrmion into a Néel bimeron, as illustrated in Fig. 4(d). In this case, the rotation of Stokes vector is more complicated. The Stokes vector performs a $\pi/2$ counterclockwise rotation around the S_2 axis, followed by a $\pi/2$ counterclockwise rotation around the S_1 axis. This rotation operation does not change the fact that the Stokes vector covers the Poincaré sphere once, so the skyrmion number remains unchanged, as confirmed by the experiment's calculated skyrmion numbers [Figs. 4(a) and 4(d)]. Helicity control can also be applied to the bimeron by replacing the PR with a WP. This adjustment is necessary because the orthogonal state of polarization comprises horizontally and vertically linearly polarized components. The experimental results align well with the corresponding theoretical predictions (see Appendix C for more experimental results).

B. Superposition of Optical Skyrmion with Different Types

In this section, we explore the superposition of optical skyrmions with different helicity or polarity, which can be achieved through the conversion of Néel skyrmions. A classical Néel skyrmion [Fig. 5(a)] was constructed by the above experimental setup and then split into two skyrmions (SK1 and SK2) of the same helicity by BS. We also modulate the helicity or polarity of the SK2, as shown in Fig. 5(b). The modulated skyrmions then pass through the next BS to synthesize a co-axis skyrmion (SK3) and superposition occurs.

First, we investigate two skyrmions with different helicity. The SK1 has a helicity of $\phi_\gamma = \phi_0$, while the SK2 has a helicity of $\phi_\gamma = \phi_0 + \Delta\phi$, which was converted by PR according to Eq. (6). It is easy to show that the superposition between two optical skyrmions with arbitrary helicity results in the intermediate skyrmion with $\phi_\gamma = \phi_0 + \Delta\phi/2$, and the orientation of the outplane changes to $s_3 = \frac{2-\rho^2(1+\cos\Delta\phi)}{2+\rho^2(1+\cos\Delta\phi)}$, which does not affect the type of skyrmion. The superposition of skyrmions with different helicity changes only the helicity, not the polarity and the vorticity. Thus, the skyrmion number remains invariant. More details on the derivation are given in Appendix D. In our experimental investigation, we initially studied the superposition of two skyrmions of the Néel type with $\phi_\gamma = 0$, as shown in Fig. 5(c). The experimental result confirmed that the output was still a Néel skyrmion with

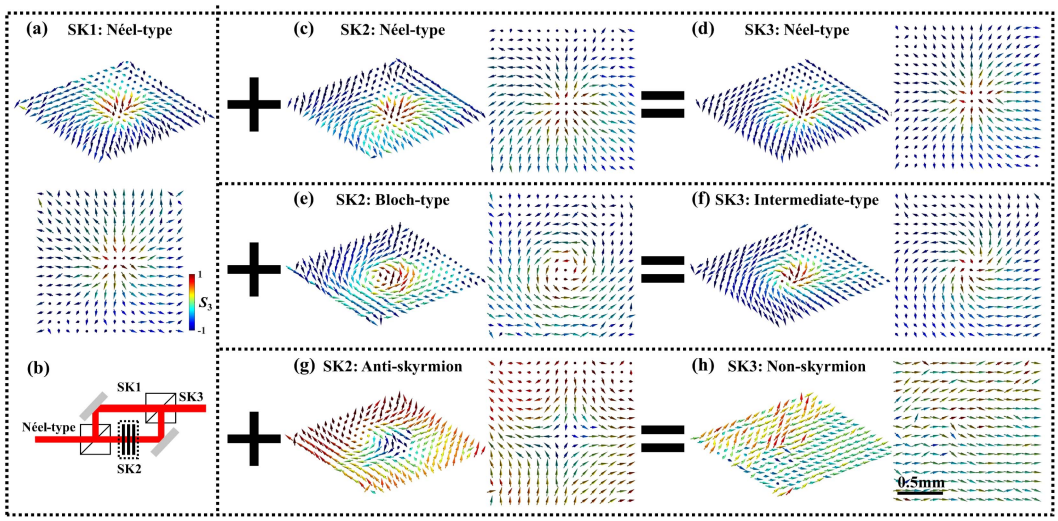

Fig. 5. Experimental results for the superposition of two optical skyrmions SK1 and SK2. (a) The same input SK1: Néel skyrmion and top view below. (b) Schematic diagram of the superposition of two optical skyrmions. Superposition with same helicity of (c) input SK2 Néel skyrmion and (d) output SK3 Néel skyrmion. Superposition with different helicity of (e) input SK2 Bloch skyrmion and (f) output SK3 intermediate skyrmion. Superposition with different polarity of (g) input SK2 antiskyrmion and (h) output SK3 nonskyrmion.

$\phi_\gamma = 0$ [see Fig. 5(d)], indicating the successful functioning of our system. Next, we proceeded to superpose Néel and Bloch ($\phi_\gamma = \pi/2$) skyrmions [Fig. 5(e)] in our experiment. The result of this superposition was an intermediate state with $\phi_\gamma = \pi/4$, as shown in Fig. 5(f). The change in the distribution of s_3 is not significant, indicating that the superposition of skyrmions with different helicity does not have a significant effect on the s_3 component of the Stokes vector.

In addition, we also investigated the superposition of two skyrmions with different polarity. Without loss of generality, we set SK1 to be of Néel type, and we convert SK2 to an antiskyrmion using an HWP according to Eq. (7). The Stokes vectors s_1 of SK1 and SK2 have the same orientation, while s_2 and s_3 have opposite orientations, as shown in Fig. 5(g). The superposition of SK1 and SK2 leads to the cancellation of s_2 and s_3, resulting in the annihilation of the skyrmion, and the formation of a nonskyrmion state with skyrmion number equal to zero, as depicted in Fig. 5(h). More experimental results are presented in detail in Appendix E.

The superposition of optical skyrmions with different types demonstrates fusion and annihilation, enabling the creation of complex and versatile structures in optical systems. This capability allows for the generation of customized light patterns with unique properties by combining skyrmions with different helicity or polarity, including controlled spin textures or the formation of nonskyrmion states. This opens possibilities for applications in high-dimensional encoding, optical information processing, and advanced imaging techniques.

4. CONCLUSION

In conclusion, we have presented a theoretical approach to accomplish the conversion among different types of skyrmionic topological textures by polarization devices. Additionally, the conversion of optical skyrmions among Néel, Bloch, antiskyrmions, and bimerons was experimentally verified by using a series of WPs. Furthermore, we have experimentally demonstrated the superposition of skyrmions with different helicity or polarity based on the proposed approach. The experimental results align with our theoretical predictions, validating the efficacy of our approach. The superposition of optical skyrmions enables the creation of complex and versatile structures in optical systems. Additionally, our scheme can be further extended to incorporate a broader range of photonic quasiparticles by leveraging the diverse designs available for WP cascades. Although the Stokes pseudovector does not adhere to the conventional rules of vector summation, the Stokes skyrmion can be effectively manipulated and transformed between different types using polarization devices. This unique property of the Stokes skyrmion has significant potential for applications in optical information processing, optical computing, and optical storage, where precise control and transformation of its properties are of utmost importance.

APPENDIX A: DETAIL OF OPTICAL SKYRMION

In this appendix, we show how to construct the skyrmion by Stokes vector and derive the skyrmion number. Optical skyrmions can be generated by superposing a pair of LG modes with orthogonal polarization states, as described in Eq. (1) of the main text. For the convenience of our analysis, we will temporarily disregard the propagation of beams. By extracting the common factorization, the Eq. (1) can be rewritten as

$$\Psi = C[\vec{e}_R + \rho e^{i\alpha(\phi)}\vec{e}_L], \tag{A1}$$

where $\rho = \tan c_0 \cdot (\frac{\sqrt{2}r}{w_0})^{|l|}; \alpha(\phi) = l\phi + \phi_\gamma; C = \cos c_0 \exp(-\frac{r^2}{w_0^2})$. It is easy to see from Eq. (A1) that the dimensionless parameter $\rho = \tan c_0 \cdot (\frac{\sqrt{2}r}{w_0})^{|l|}$ regulates the ratio of the two polarizations, so that the polarization approaches $\vec{e}_R$, as it gets closer to the axis, and approaches $\vec{e}_L$, as it moves away from it. To ensure

that the significant intensity region of the beam, the width of the beam w, encompasses most polarizations, it is desirable to select a value for c_0 such that $\tan c_0$ is of the order of unity.

The skyrmion vector field is constructed by Stokes vector, so we need to calculate the field configuration of Stokes parameters of beam, which can be expressed as

$$S = \begin{pmatrix} |E_R|^2 + |E_L|^2 \\ 2\,\mathrm{Re}(E_R E_L^*) \\ -2\,\mathrm{Im}(E_R E_L^*) \\ |E_R|^2 - |E_L|^2 \end{pmatrix} = C^2 \begin{pmatrix} 1+\rho^2 \\ 2\rho\cos\alpha(\phi) \\ 2\rho\sin\alpha(\phi) \\ 1-\rho^2 \end{pmatrix} = C^2(1+\rho^2) \begin{pmatrix} 1 \\ \frac{2\rho}{1+\rho^2}\cos\alpha(\phi) \\ \frac{2\rho}{1+\rho^2}\sin\alpha(\phi) \\ \frac{1-\rho^2}{1+\rho^2} \end{pmatrix}. \tag{A2}$$

According to Pythagorean theorem $\cos\beta(\rho) = \frac{2\rho}{1+\rho^2}$ and $\sin\beta(\rho) = \frac{1-\rho^2}{1+\rho^2}$, the normalized reduced Stokes vector can be given by

$$\vec{s} = \begin{pmatrix} \cos\beta(\rho)\cos\alpha(\phi) \\ \cos\beta(\rho)\sin\alpha(\phi) \\ \sin\beta(\rho) \end{pmatrix}, \tag{A3}$$

where $\alpha(\phi) = l\phi + \phi_\gamma$. Equation (A3) describes the Stokes vector configuration of Eq. (1), which corresponds to the skyrmion texture. The topological property of an optical skyrmion is determined by the skyrmion number, as described in Eq. (3) of the main text. Exploiting the radial symmetry, the skyrmion number can be derived as

$$\begin{aligned} s &= \frac{1}{4\pi}\iint_\sigma \vec{n}\cdot\left(\frac{\partial\vec{n}}{\partial x}\times\frac{\partial\vec{n}}{\partial y}\right)\mathrm{d}x\mathrm{d}y \\ &= \frac{1}{4\pi}\int_0^{r_\sigma}\mathrm{d}r\int_0^{2\pi}\mathrm{d}\phi\frac{\mathrm{d}\beta(r)}{\mathrm{d}r}\frac{\mathrm{d}\alpha(\phi)}{\mathrm{d}\phi}\sin\beta(r) \\ &= \frac{1}{2}[\sin\beta(r)]_{r=0}^{r=r_\sigma}\cdot\frac{1}{2\pi}[\alpha(\phi)]_{\phi=0}^{\phi=2\pi} \\ &= p\cdot m, \end{aligned} \tag{A4}$$

where $p = \frac{1}{2}[\sin\beta(r)]_{r=0}^{r=r_\sigma}$ and $m = \frac{1}{2\pi}[\alpha(\phi)]_{\phi=0}^{\phi=2\pi}$, which represent the vertical and horizontal wrapping times.

APPENDIX B: FUNDAMENTAL THEORY OF THE SKYRMION CONVERSION

In this appendix, we will delve into the effects of the WP on skyrmions, providing a detailed analysis of its influence on these optical quasiparticles. The Stokes vector configuration of skyrmion can be represented as $(s_1, s_2, s_3)^T$, allowing us to describe the effect of the WP on the skyrmion using Mueller matrices.

First, we consider the action of the WP with fast axis horizontal with a phase delay ϕ, and the Mueller matrix can be expressed as

$$M_{\mathrm{WP}}(\phi) = \begin{bmatrix} 1 & 0 & 0 \\ 0 & \cos\phi & -\sin\phi \\ 0 & \sin\phi & \cos\phi \end{bmatrix}. \tag{B1}$$

We observe that the matrix corresponds to a rotation matrix with the S_1 direction as the rotation axis, and the rotation angle is determined by the phase delay. However, it is important to note that, if the fast axis is chosen to be the S_2 direction instead, the rotation direction will be reversed.

Then, we consider the action of the WP with fast axis $\pi/4$ with a phase delay ϕ, and the Mueller matrix can be written as

$$M_{\mathrm{WP}}(\phi) = \begin{bmatrix} \cos\phi & 0 & \sin\phi \\ 0 & 1 & 0 \\ -\sin\phi & 0 & \cos\phi \end{bmatrix}. \tag{B2}$$

We found that this matrix also corresponds to the rotation matrix, except that the axis of rotation has changed from the S_1 direction to the S_2 direction.

Finally, we consider the action of the WP with fast axis θ with a phase delay ϕ, and the Mueller matrix is found to be

$$M_{\mathrm{WP}}(\phi) = \begin{bmatrix} \cos^2 2\theta + \cos\phi\sin^2 2\theta & (1-\cos\phi)\sin 2\theta\cos 2\theta & \sin\phi\sin 2\theta \\ (1-\cos\phi)\sin 2\theta\cos 2\theta & \sin^2 2\theta + \cos\phi\cos^2 2\theta & -\sin\phi\cos 2\theta \\ \sin\phi\sin 2\theta & \sin\phi\cos 2\theta & \cos\phi \end{bmatrix}. \tag{B3}$$

This matrix also corresponds to the rotation matrix, except that the axis of rotation has changed from the S_1 direction to the 2θ direction. It should be noted that the rotation axis of this rotation matrix is limited to the S_1–S_2 plane. As a result, a single waveplate is unable to achieve rotation along the S_3 direction.

In order to achieve rotation around the S_3 direction, we need to combine a series of WPs, e.g., by combining two HWPs [34] or by combining two QWPs and a retarder with a phase shift ϕ [43]. In the following, we demonstrate the latter approach, and the corresponding Mueller matrix can be expressed as

$$\begin{aligned} M &= \mathrm{QWP}(0)\mathrm{WP}(\phi,\pi/4)\mathrm{QWP}(\pi/2) \\ &= \begin{bmatrix} 1 & 0 & 0 \\ 0 & 0 & 1 \\ 0 & -1 & 0 \end{bmatrix}\begin{bmatrix} \cos\phi & 0 & -\sin\phi \\ 0 & 1 & 0 \\ \sin\phi & 0 & \cos\phi \end{bmatrix}\begin{bmatrix} 1 & 0 & 0 \\ 0 & 0 & -1 \\ 0 & 1 & 0 \end{bmatrix} \\ &= \begin{bmatrix} \cos\phi & -\sin\phi & 0 \\ \sin\phi & \cos\phi & 0 \\ 0 & 0 & 1 \end{bmatrix}. \end{aligned} \tag{B4}$$

Thus far, we have successfully implemented rotations around the S_1, S_2, and S_3 directions. A WP will induce a

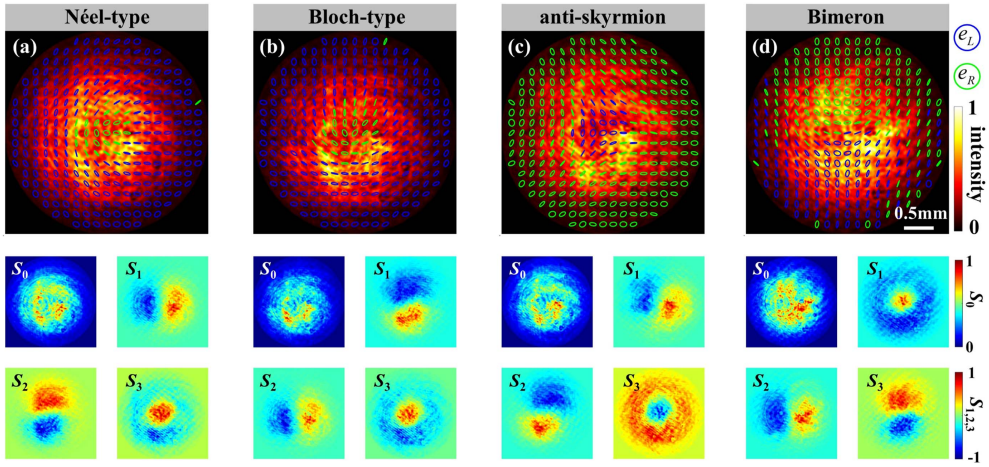

Fig. 6. More experimental results for optical skyrmion conversion. (a) The intensity, state of polarization distribution of input Néel skyrmion, and corresponding Stokes components below. Output intensity, state of polarization distribution of (b) Bloch skyrmion converted by PR, (c) antiskyrmion with $p = -1$ converted by HWP, and (d) bimeron converted by two QWPs with corresponding Stokes components below.

uniform rotation in all Stokes vectors of skyrmions. For instance, a rotation along the S_3 direction alters the helicity of the skyrmion, a π rotation along the S_1 direction results in an antiskyrmion with $p = -1$, and a $\pi/2$ rotation along the S_1 direction followed by a $\pi/2$ rotation along the S_2 direction leads to a bimeron.

APPENDIX C: MORE EXPERIMENTAL RESULTS OF SKYRMION CONVERSION

In this appendix, we present more detailed experimental results of skyrmion conversion to complement the main text. While the main text focuses on demonstrating three specific transformations of the skyrmion in terms of the Stokes vector, here we provide additional information of skyrmion conversion, including the intensity field distribution, polarization state distribution, and the three components of the Stokes vector, as shown in Fig. 6.

APPENDIX D: THEORY OF SUPERPOSITION OF DIFFERENT SKYRMIONS

In this appendix, we present the detail theory of the superposition of a skyrmion with different types. First, we investigate the superposition between two optical skyrmions (SK1 with $\phi_\gamma = \phi_0$ and SK2 with $\phi_\gamma = \phi_0 + \Delta\phi$) with arbitrary helicity, which can be written as

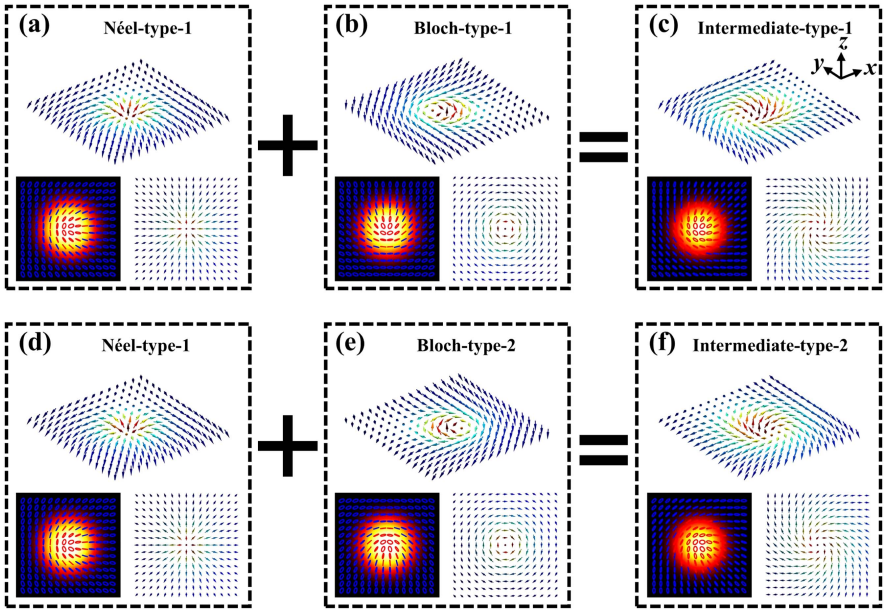

Fig. 7. First row is the Stokes vector distribution, intensity with polarization distributions and transverse component of Stokes vector of the input SK1 Néel-type-1 with $\phi_\gamma = 0$ (a) and SK2 Bloch-type with $\phi_\gamma = \pi/2$ (b), and output SK3 intermediate-type with $\phi_\gamma = \pi/4$ (c). Second row corresponds to SK1 Néel-type-1 with $\phi_\gamma = 0$ (d) and SK2 Bloch-type with $\phi_\gamma = -\pi/2$ (e), and output SK3 intermediate-type with $\phi_\gamma = -\pi/4$ (f).

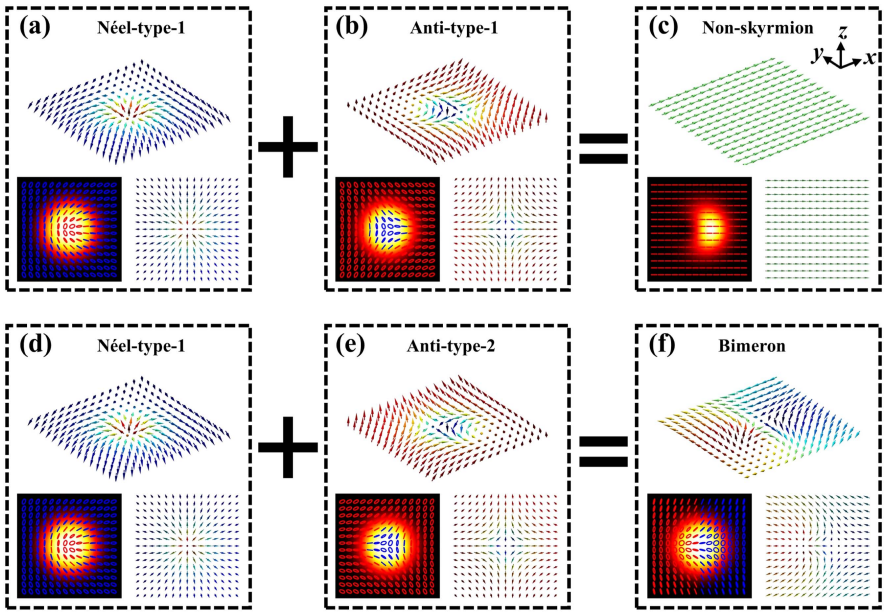

Fig. 8. First row is the Stokes vector distribution, intensity with polarization distributions and transverse component of Stokes vector of the input SK1 Néel-type-1 with $\phi_\gamma = 0$ (a) and SK2 antitype with $p = -1, \phi_\gamma = 0$ (b), and output SK3 nonskyrmion (c). Second row corresponds to SK1 Néel -type-1 with $\phi_\gamma = 0$ (d) and SK2 antitype-2 with $p = -1, \phi_\gamma = \pi$ (e), and output SK3 bimeron (f).

$$\mathrm{SK1} = \cos c_0 \cdot \mathrm{LG}_{0,0} \cdot \vec{e}_R + \sin c_0 \cdot e^{i\phi_0} \mathrm{LG}_{0,1} \cdot \vec{e}_L,$$
$$\mathrm{SK2} = \cos c_0 \cdot \mathrm{LG}_{0,0} \cdot \vec{e}_R + \sin c_0 \cdot e^{i(\phi_0+\Delta\phi)} \mathrm{LG}_{0,1} \cdot \vec{e}_L. \quad \textbf{(D1)}$$

These normalized Stokes vectors can be derived as follows:

$$\vec{s} = \begin{pmatrix} \cos\beta\, \cos(\phi + \phi_0 + \Delta\phi/2) \\ \cos\beta\, \sin(\phi + \phi_0 + \Delta\phi/2) \\ \sin\beta \end{pmatrix}, \quad \textbf{(D2)}$$

where $\cos\beta = \frac{2\rho(1+\cos\Delta\phi)}{2+\rho^2(1+\cos\Delta\phi)}$ and $\sin\beta = \frac{2-\rho^2(1+\cos\Delta\phi)}{2+\rho^2(1+\cos\Delta\phi)}$.

Equation (D2) shows that the superposition between two optical skyrmions with arbitrary helicity can also result in the intermediate skyrmion type with $\phi_\gamma = \phi_0 + \Delta\phi/2$ and slightly changes of the distribution of s_3. Figure 7 shows the superposition between Néel- and Bloch-type. The first row shows the superposition between Néel-type-1 with $\phi_\gamma = 0$ and Bloch-type-1 with $\phi_\gamma = \pi/2$ and results in the intermediate-type-1 with $\phi_\gamma = \pi/4$, as shown in Figs. 7(a)–7(c). The second row shows the superposition between Néel-type-1 with $\phi_\gamma = 0$ and Bloch-type-2 with $\phi_\gamma = -\pi/2$ and results in the intermediate-type-2 with $\phi_\gamma = -\pi/4$, as shown in Figs. 7(d)–7(f).

Next, we investigate the superposition of optical skyrmions with opposite polarity but arbitrary helicity. The field configuration of these optical skyrmions can be expressed as

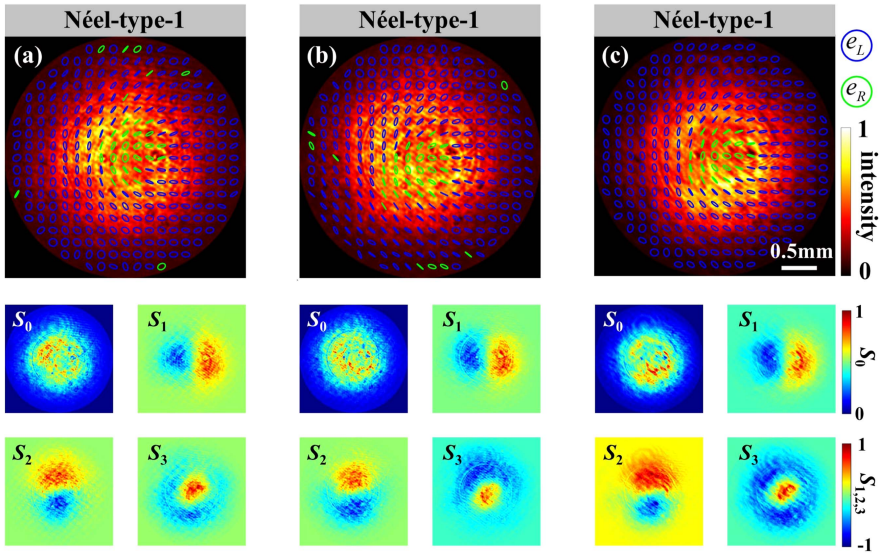

Fig. 9. More experimental results for superposition of Néel-type-1 and Néel-type-1. (a) Intensity with state of polarization distribution and Stokes components of input SK1 Néel-type-1. (b) corresponds to the input SK2 Néel-type-1. (c) corresponds to the output SK3 Néel-type-1.

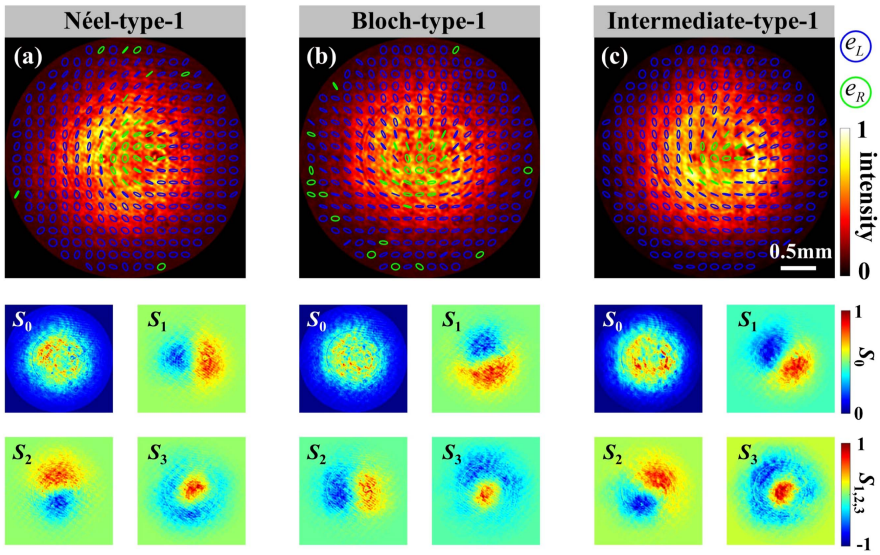

Fig. 10. More experimental results for superposition of Néel-type-1 and Bloch-type-1. (a) Intensity with state of polarization distribution and Stokes components of input SK1 Néel-type-1. (b) corresponds to the input SK2 Bloch-type-1. (c) corresponds to the output SK3 intermediate-type-1.

$$\mathrm{SK1} = \cos\, c_0 \cdot \mathrm{LG}_{0,0} \cdot \vec{e}_R + \sin\, c_0 \cdot e^{i\phi_0} \mathrm{LG}_{0,1} \cdot \vec{e}_L,$$
$$\mathrm{SK2} = \cos\, c_0 \cdot \mathrm{LG}_{0,0} \cdot \vec{e}_L + \sin\, c_0 \cdot e^{i(\phi_0+\Delta\phi)} \mathrm{LG}_{0,1} \cdot \vec{e}_R. \quad \textbf{(D3)}$$

The normalized Stokes vector of the superposition can be calculated as follows:

$$\vec{s} = \begin{pmatrix} \dfrac{1+\rho^2\cos\Delta\phi+2\rho\cos\Delta\phi/2\cos(\phi+\phi_0+\Delta\phi/2)}{1+\rho^2+2\rho\cos\Delta\phi/2\cos(\phi+\phi_0+\Delta\phi/2)} \\ -\dfrac{\rho^2\sin\Delta\phi+2\rho\sin\Delta\phi/2\cos(\phi+\phi_0+\Delta\phi/2)}{1+\rho^2+2\rho\cos\Delta\phi/2\cos(\phi+\phi_0+\Delta\phi/2)} \\ -\dfrac{2\rho\sin\Delta\phi/2\sin(\phi+\phi_0+\Delta\phi/2)}{1+\rho^2+2\rho\cos\Delta\phi/2\cos(\phi+\phi_0+\Delta\phi/2)} \end{pmatrix}. \quad \textbf{(D4)}$$

For the superposition of skyrmions with opposite polarity [they also have opposite vorticity according to Eq. (7)], the vector distribution of SK3 described in Eq. (D4) is not sufficiently elegant. From Eq. (D4), we cannot determine their topological properties, but we find two special cases with interesting topologies. One is the nonskyrmion; the other is the bimeron topology. As $\Delta\phi = 0$, the distribution of its normalized Stokes vector can be written as

$$\vec{s}(\Delta\phi = 0) = \begin{pmatrix} 1 \\ 0 \\ 0 \end{pmatrix}. \quad \textbf{(D5)}$$

It is evident from the equation above that the Stokes vector has only one direction in space, aligned with S_1, as shown in

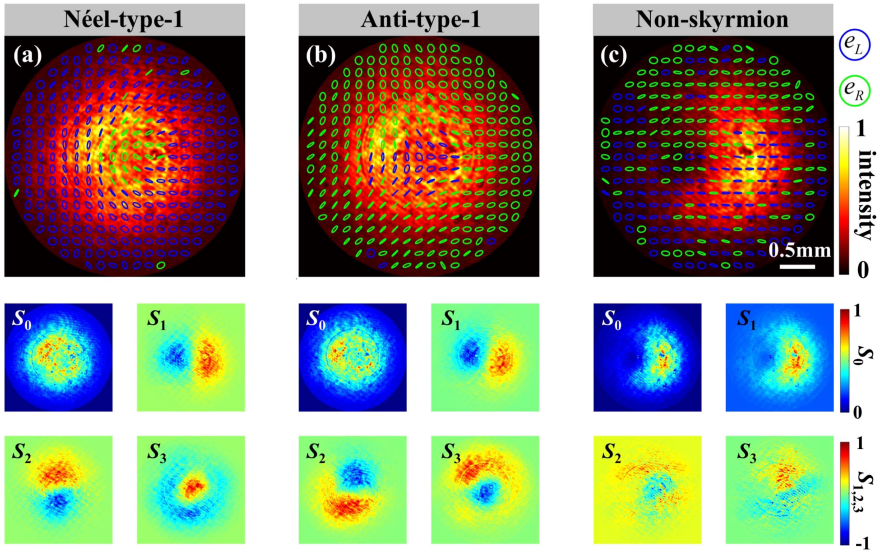

Fig. 11. More experimental results for superposition of Néel-type-1 and antitype-1. (a) Intensity with state of polarization distribution and Stokes components of input SK1 Néel-type-1. (b) corresponds to the input SK2 antitype-1. (c) corresponds to the output SK3 nonskyrmion.

Figs. 8(a)–8(c). Clearly, this represents a trivial topology, and the skyrmion number is zero.

As $\Delta\phi = \pi$, we can obtain the topology of a bimeron [see Figs. 8(d)–8(f)], whose normalized Stokes vector distribution can be expressed as

$$\vec{s}(\Delta\phi = \pi) = \begin{pmatrix} \sin\beta \\ -\cos\beta\,\cos(\phi + \phi_0 + \pi/2) \\ -\cos\beta\,\sin(\phi + \phi_0 + \pi/2) \end{pmatrix}, \quad \textbf{(D6)}$$

where $\cos\beta = \frac{2\rho}{1+\rho^2}$ and $\sin\beta = \frac{1-\rho^2}{1+\rho^2}$. From the above equations, we can observe that the distribution of the Stokes vector is similar to Eq. (9) in the main text, with the only difference being that s_2 and s_3 have a negative sign, corresponding to a phase change of π in helicity. Furthermore, using a similar approach, we can deduce that the bimeron has a polarity of 1, vorticity of 1, and helicity of π. The skyrmion number is also equal to 1.

APPENDIX E: MORE EXPERIMENTAL RESULTS OF SUPERPOSITION OF DIFFERENT SKYRMIONS

In this appendix, we present more detailed experimental results of Fig. 5 in the main text. Figure 9 shows the intensity field distribution, polarization state distribution, and the three components of the Stokes vector for the superposition between Néel-type-1 and Néel-type-1. Figures 10 and 11 show the superposition between Néel-type-1 and Bloch-type-1 and between Néel-type-1 and antitype-1, respectively.

Funding. National Natural Science Foundation of China (92050202, 12204309); Shanghai Rising-Star Program (22YF1415200, 23YF1415800).

Disclosures. The authors declare no competing interests.

Data Availability. The data that support the findings of this study are available from the corresponding author upon reasonable request.

REFERENCES

1. B. Göbel, I. Mertig, and O. A. Tretiakov, "Beyond skyrmions: review and perspectives of alternative magnetic quasiparticles," Phys. Rep. **895**, 1–28 (2021).
2. N. Nagaosa and Y. Tokura, "Topological properties and dynamics of magnetic skyrmions," Nat. Nanotechnol. **8**, 899–911 (2013).
3. S. Mühlbauer, B. Binz, F. Jonietz, C. Pfleiderer, A. Rosch, A. Neubauer, R. Georgii, and P. Böni, "Skyrmion lattice in a chiral magnet," Science **323**, 915–919 (2009).
4. X. Z. Yu, Y. Onose, N. Kanazawa, J. H. Park, J. H. Han, Y. Matsui, N. Nagaosa, and Y. Tokura, "Real-space observation of a two-dimensional skyrmion crystal," Nature **465**, 901–904 (2010).
5. D. Foster, C. Kind, P. J. Ackerman, J. S. B. Tai, M. R. Dennis, and I. I. Smalyukh, "Two-dimensional skyrmion bags in liquid crystals and ferromagnets," Nat. Phys. **15**, 655–659 (2019).
6. S. Tsesses, E. Ostrovsky, K. Cohen, B. Gjonaj, N. H. Lindner, and G. Bartal, "Optical skyrmion lattice in evanescent electromagnetic fields," Science **361**, 993–996 (2018).
7. T. J. Davis, D. Janoschka, P. Dreher, B. Frank, F.-J. M. Z. Heringdorf, and H. Giessen, "Ultrafast vector imaging of plasmonic skyrmion dynamics with deep subwavelength resolution," Science **368**, eaba6415 (2020).
8. L. Du, A. Yang, A. V. Zayats, and X. Yuan, "Deep-subwavelength features of photonic skyrmions in a confined electromagnetic field with orbital angular momentum," Nat. Phys. **15**, 650–654 (2019).
9. X. Lei, A. Yang, P. Shi, Z. Xie, L. Du, A. V. Zayats, and X. Yuan, "Photonic spin lattices: symmetry constraints for skyrmion and meron topologies," Phys. Rev. Lett. **127**, 237403 (2021).
10. X. Lei and Q. Zhan, "Topological charge constrained photonic skyrmion defects in split plasmonic vortices," ACS Photon. **10**, 3551–3557 (2023).
11. X. Lei, L. Du, X. Yuan, and Q. Zhan, "Metastability of photonic spin meron lattices in the presence of perturbed spin-orbit coupling," Opt. Express **31**, 2225–2233 (2023).
12. Y. Dai, Z. Zhou, A. Ghosh, R. S. K. Mong, A. Kubo, C. B. Huang, and H. Petek, "Plasmonic topological quasiparticle on the nanometre and femtosecond scales," Nature **588**, 616–619 (2020).
13. Y. Dai, Z. Zhou, A. Ghosh, K. Kapoor, M. Dąbrowski, A. Kubo, C. B. Huang, and H. Petek, "Ultrafast microscopy of a twisted plasmonic spin skyrmion," Appl. Phys. Rev. **9**, 011420 (2022).
14. Z. L. Deng, T. Shi, A. Krasnok, X. Li, and A. Alù, "Observation of localized magnetic plasmon skyrmions," Nat. Commun. **13**, 8 (2022).
15. J. Yang, X. Zheng, J. Wang, Y. Pan, A. Zhang, T. J. Cui, and G. A. E. Vandenbosch, "Symmetry-protected spoof localized surface plasmonic skyrmion," Laser Photon. Rev. **16**, 2200007 (2022).
16. C. Bai, J. Chen, Y. Zhang, D. Zhang, and Q. Zhan, "Dynamic tailoring of an optical skyrmion lattice in surface plasmon polaritons," Opt. Express **28**, 10320–10328 (2020).
17. R. Gutiérrez-Cuevas and E. Pisanty, "Optical polarization skyrmionic fields in free space," J. Opt. **23**, 024004 (2021).
18. S. Gao, F. C. Speirits, F. Castellucci, S. Franke-Arnold, S. M. Barnett, and J. B. Götte, "Paraxial skyrmionic beams," Phys. Rev. A **102**, 053513 (2020).
19. Y. Shen, E. C. Martínez, and C. Rosales-Guzmán, "Generation of optical skyrmions with tunable topological textures," ACS Photon. **9**, 296–303 (2022).
20. Y. Shen, C. He, Z. Song, B. Chen, H. He, Y. Ma, J. A. J. Fells, S. J. Elston, S. M. Morris, M. J. Booth, and A. Forbes, "Topologically controlled multiskyrmions in photonic gradient-index lenses," arXiv, arXiv:2304.06332 (2023).
21. C. Cisowski, C. Ross, and S. Franke-Arnold, "Building paraxial optical skyrmions using rational maps," Adv. Photon. Res. **4**, 2200350 (2023).
22. K. Singh, P. Ornelas, A. Dudley, and A. Forbes, "Synthetic spin dynamics with Bessel-Gaussian optical skyrmions," Opt. Express **31**, 15289–15300 (2023).
23. W. Lin, Y. Ota, Y. Arakawa, and S. Iwamoto, "Microcavity-based generation of full Poincaré beams with arbitrary skyrmion numbers," Phys. Rev. Res. **3**, 023055 (2021).
24. A. Karnieli, S. Tsesses, G. Bartal, and A. Arie, "Emulating spin transport with nonlinear optics, from high-order skyrmions to the topological Hall effect," Nat. Commun. **12**, 1092 (2021).
25. X. Luo, Y. Cai, X. Yue, W. Lin, J. Zhu, Y. Zhang, and F. Li, "Non-Hermitian control of confined optical skyrmions in microcavities formed by photonic spin–orbit coupling," Photon. Res. **11**, 610–621 (2023).
26. M. Król, H. Sigurdsson, K. Rechcińska, P. Oliwa, K. Tyszka, W. Bardyszewski, A. Opala, M. Matuszewski, P. Morawiak, R. Mazur, W. Piecek, P. Kula, P. G. Lagoudakis, B. Piętka, and J. Szczytko, "Observation of second-order meron polarization textures in optical microcavities," Optica **8**, 255–261 (2021).
27. Y. Shen, Q. Zhang, P. Shi, L. Du, A. V. Zayats, and X. Yuan, "Topological quasiparticles of light: optical skyrmions and beyond," arXiv, arXiv:2205.10329 (2022).
28. Y. Shen, "Topological bimeronic beams," Opt. Lett. **46**, 3737–3740 (2021).
29. Y. Shen, Y. Hou, N. Papasimakis, and N. I. Zheludev, "Supertoroidal light pulses as electromagnetic skyrmions propagating in free space," Nat. Commun. **12**, 5891 (2021).
30. A. Zdagkas, C. McDonnell, J. Deng, Y. Shen, G. Li, T. Ellenbogen, N. Papasimakis, and N. I. Zheludev, "Observation of toroidal pulses of light," Nat. Photonics **16**, 523–528 (2022).
31. X. Lei, L. Du, X. Yuan, and A. V. Zayats, "Optical spin–orbit coupling in the presence of magnetization: photonic skyrmion interaction with magnetic domains," Nanophotonics **10**, 3667–3675 (2021).

32. A. Yang, X. Lei, P. Shi, F. Meng, M. Lin, L. Du, and X. Yuan, "Spin-manipulated photonic skyrmion-pair for pico-metric displacement sensing," Adv. Sci. **10**, 2205249 (2023).
33. Y. Shen, B. Yu, H. Wu, C. Li, Z. Zhu, and A. V. Zayats, "Topological transformation and free-space transport of photonic hopfions," Adv. Photon. **5**, 015001 (2023).
34. R. Simon and N. Mukunda, "Universal SU(2) gadget for polarization optics," Phys. Lett. A **138**, 474–480 (1989).
35. R. Simon and N. Mukunda, "Minimal three-component SU(2) gadget for polarization optics," Phys. Lett. A **143**, 165–169 (1990).
36. A. M. Beckley, T. G. Brown, and M. A. Alonso, "Full Poincaré beams," Opt. Express **18**, 10777–10785 (2010).
37. A. E. Siegman, *Lasers* (University Science Books, 1986).
38. O. A. Tretiakov and O. Tchernyshyov, "Vortices in thin ferromagnetic films and the skyrmion number," Phys. Rev. B **75**, 012408 (2007).
39. I. Kézsmárki, S. Bordács, P. Milde, E. Neuber, L. M. Eng, J. S. White, H. M. Rønnow, C. D. Dewhurst, M. Mochizuki, K. Yanai, H. Nakamura, D. Ehlers, V. Tsurkan, and A. Loidl, "Néel-type skyrmion lattice with confined orientation in the polar magnetic semiconductor GaV_4S_8," Nat. Mater. **14**, 1116–1122 (2015).
40. D. A. Gilbert, B. B. Maranville, A. L. Balk, B. J. Kirby, P. Fischer, D. T. Pierce, J. Unguris, J. A. Borchers, and K. Liu, "Realization of ground-state artificial skyrmion lattices at room temperature," Nat. Commun. **6**, 8462 (2015).
41. P. Milde, D. Köhler, J. Seidel, L. M. Eng, A. Bauer, A. Chacon, J. Kindervater, S. Mühlbauer, C. Pfleiderer, S. Buhrandt, C. Schütte, and A. Rosch, "Unwinding of a skyrmion lattice by magnetic monopoles," Science **340**, 1076–1080 (2013).
42. A. K. Nayak, V. Kumar, T. Ma, P. Werner, E. Pippel, R. Sahoo, F. Damay, U. K. Rößler, C. Felser, and S. S. P. Parkin, "Magnetic anti-skyrmions above room temperature in tetragonal Heusler materials," Nature **548**, 561–566 (2017).
43. C. Ye, "Construction of an optical rotator using quarter-wave plates and an optical retarder," Opt. Eng. **34**, 3031–3035 (1995).
44. W. Han, Y. Yang, W. Cheng, and Q. Zhan, "Vectorial optical field generator for the creation of arbitrarily complex fields," Opt. Express **21**, 20692–20706 (2013).
45. A. McWilliam, C. M. Cisowski, Z. Ye, F. C. Speirits, J. B. Götte, S. M. Barnett, and S. Franke-Arnold, "Topological approach of characterizing optical skyrmions and multi-skyrmions," Laser Photon. Rev. **17**, 2300155 (2023).